

5. Silicon Vertex Tracker

5.1. Charged Particle Tracking

The principal purpose of the *BABAR* charged particle tracking systems, the SVT and the DCH, is the efficient detection of charged particles and the measurement of their momentum and angles with high precision. Among many applications, these precision measurements allow for the reconstruction of exclusive B - and D -meson decays with high resolution and thus minimal background. The reconstruction of multiple decay vertices of weakly decaying B and D mesons is of prime importance to the physics goals.

Track measurements are also important for the extrapolation to the DIRC, EMC, and IFR. At lower momenta, the DCH measurements are more important, while at higher momenta the SVT measurements dominate. Most critical are the angles at the DIRC, because the uncertainties in the charged particle track parameters add to the uncertainty in the measurement of the Cherenkov angle. Thus, the track errors from the combined SVT and DCH measurements should be small compared to the average DIRC Cherenkov angle measurements, *i.e.*, of order of 1 mrad, particularly at the highest momenta.

5.2. SVT Goals and Design Requirements

The SVT has been designed to provide precise reconstruction of charged particle trajectories and decay vertices near the interaction region. The design choices were driven primarily by direct requirements from physics measurements and constraints imposed by the PEP-II interaction region and *BABAR* experiment. In this section the mechanical and electronic design of the SVT are discussed, with some discussion of the point resolution per layer and dE/dx performance. The tracking performance and efficiency of the SVT alone and in combination with the DCH are described in Section 7.

5.2.1. SVT Requirements and Constraints

The SVT is critical for the measurement of the time-dependent CP asymmetry. To avoid significant impact of the resolution on the CP asymmetry measurement the mean vertex resolution along the z -axis for a fully reconstructed B de-

cah must be better than $80 \mu\text{m}$ [2]. The required resolution in the x - y plane arises from the need to reconstruct final states in B decays as well as in τ and charm decays. For example, in decays of the type $B^0 \rightarrow D^+ D^-$, separating the two D vertices is important. The distance between the two D 's in the x - y plane for this decay is typically $\sim 275 \mu\text{m}$. Hence, the SVT needs to provide resolution of order $\sim 100 \mu\text{m}$ in the plane perpendicular to the beam line.

Many of the decay products of B mesons have low p_t . The SVT must provide standalone tracking for particles with transverse momentum less than $120 \text{ MeV}/c$, the minimum that can be measured reliably in the DCH alone. This feature is fundamental for the identification of slow pions from D^* -meson decays: a tracking efficiency of 70% or more is desirable for tracks with a transverse momentum in the range 50 – $120 \text{ MeV}/c$. The standalone tracking capability and the need to link SVT tracks to the DCH were crucial in choosing the number of layers.

Beyond the standalone tracking capability, the SVT provides the best measurement of track angles, which is required to achieve design resolution for the Cherenkov angle for high momentum tracks.

Additional constraints are imposed by the storage ring components. The SVT is located inside the ~ 4.5 -m-long support tube, that extends all the way through the detector. To maximize the angular coverage, the SVT must extend down to 350 mrad (20°) in polar angle from the beam line in the forward direction. The region at smaller polar angles is occupied by the B1 permanent magnets. In the backward direction, it is sufficient to extend the SVT sensitive area down to 30° .

The SVT must withstand 2 MRad of ionizing radiation. A radiation monitoring system capable of aborting the beams is required. The expected radiation dose is 1 Rad/day in the horizontal plane immediately outside the beam pipe (where the highest radiation is concentrated), and 0.1 Rad/day on average otherwise.

The SVT is inaccessible during normal detector operations. Hence, reliability and robustness are essential: all components of the SVT inside

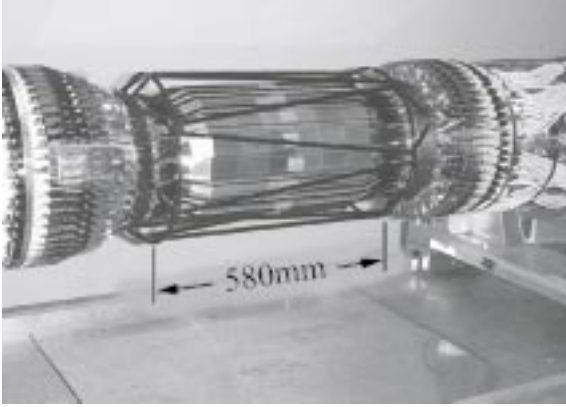


Figure 16. Fully assembled SVT. The silicon sensors of the outer layer are visible, as is the carbon-fiber space frame (black structure) that surrounds the silicon.

the support tube should have long mean-time-to-failure, because the time needed for any replacement is estimated to be 4–5 months. Redundancies are built in whenever possible and practical.

The SVT is cooled to remove the heat generated by the electronics. In addition, it operates in the 1.5 T magnetic field.

To achieve the position resolution necessary to carry out physics analyses, the relative position of the individual silicon *sensors* should be stable over long time periods. The assembly allows for relative motion of the support structures with respect to the B1 magnets.

These requirements and constraints have led to the choice of a SVT made of five layers of double-sided silicon strip sensors. To fulfill the physics requirements, the spatial resolution, for perpendicular tracks, must be 10–15 μm in the three inner layers and about 40 μm in the two outer layers. The inner three layers perform the impact parameter measurements, while the outer layers are necessary for pattern recognition and low p_t tracking.

5.3. SVT Layout

The five layers of double-sided silicon strip sensors, which form the SVT detector, are organized in 6, 6, 6, 16, and 18 modules, respectively; a photograph is shown in Figure 16. The strips on the opposite sides of each sensor are oriented orthog-

onally to each other: the ϕ measuring strips (ϕ strips) run parallel to the beam and the z measuring strips (z strips) are oriented transversely to the beam axis. The modules of the inner three layers are straight, while the modules of layers 4 and 5 are *arch-shaped* (Figures 17 and 18).

This arch design was chosen to minimize the amount of silicon required to cover the solid angle, while increasing the crossing angle for particles near the edges of acceptance. A photograph of an outer layer arch module is shown in Figure 19. The modules are divided electrically into two half-modules, which are read out at the ends.

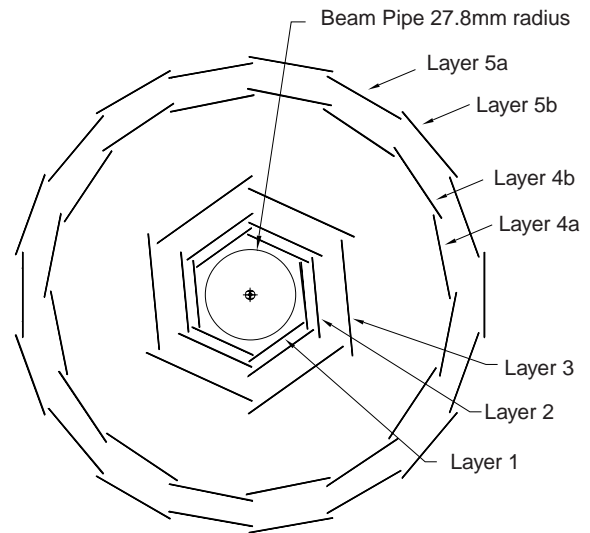


Figure 18. Schematic view of SVT: transverse section.

To satisfy the different geometrical requirements of the five SVT layers, five different sensor shapes are required to assemble the planar sections of the layers. The smallest detectors are $43 \times 42 \text{ mm}^2$ ($z \times \phi$), and the largest are $68 \times 53 \text{ mm}^2$. Two identical trapezoidal sensors are added (one each at the forward and backward ends) to form the arch modules. The half-modules are given mechanical stiffness by means of two carbon fiber/kevlar ribs, which are visible in Figure 19. The ϕ strips of sensors in the same half-module are electrically connected with wire

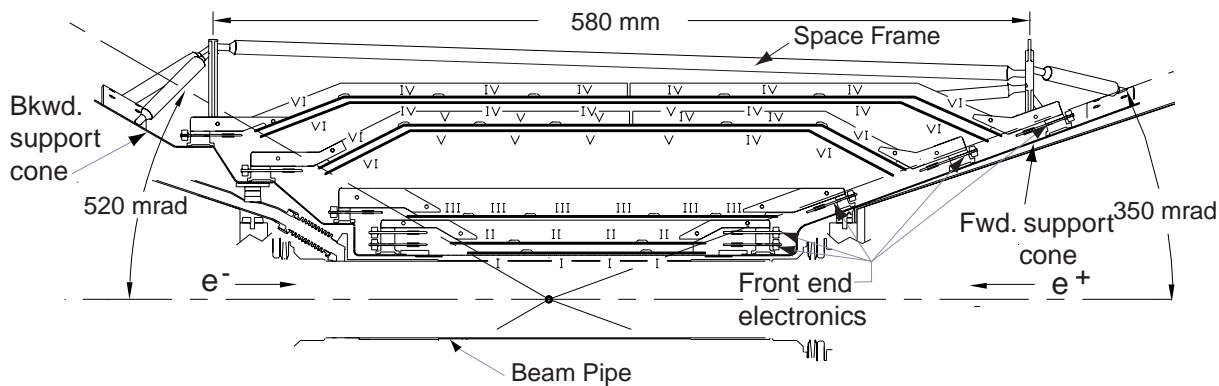


Figure 17. Schematic view of SVT: longitudinal section. The roman numerals label the six different types of sensors.

bonds to form a single readout strip. This results in a total strip length up to 140 mm (240 mm) in the inner (outer) layers.

The signals from the z strips are brought to the readout electronics using fanout circuits consisting of conducting traces on a thin ($50\ \mu\text{m}$) insulating Upilex [33] substrate. For the innermost three layers, each z strip is connected to its own preamplifier channel, while in layers 4 and 5 the number of z strips on a half-module exceeds the number of electronics channels available, requiring that two z strips on different sensors be electrically connected (ganged) to a single electronics channel. The length of a z strip is about 50 mm (no ganging) or 100 mm (two strips connected). The ganging introduces an ambiguity on the z coordinate measurement, which must be resolved by the pattern recognition algorithms. The total number of readout channels is approximately 150,000.

The inner modules are tilted in ϕ by 5° , allowing an overlap region between adjacent modules, a feature that provides full azimuthal coverage and is advantageous for alignment. The outer modules cannot be tilted, because of the arch geometry. To avoid gaps and to have a suitable overlap in the ϕ coordinate, layers 4 and 5 are divided into two sub-layers (4a, 4b, 5a, 5b) and placed at slightly different radii (see Figure 18). The relevant geometrical parameters of each layer



Figure 19. Photograph of an SVT arch module in an assembly jig.

are summarized in Table 5.

Table 5

Geometric parameters for each layer and readout plane of the SVT. Floating strips refers to the number of strips between readout (R-O) strips. Note: parts of the ϕ sides of layers 1 and 2 are bonded at 100 μm and 110 μm pitch, respectively, with one floating strip. Strip length of z -strips for layers 4 and 5 includes ganging. The radial range for layers 4 and 5 includes the radial extent of the arched sections.

Layer/ view	Radius (mm)	R-O pitch (μm)	Floating strips	Strip length (mm)
1 z	32	100	1	40
1 ϕ	32	50-100	0-1	82
2 z	40	100	1	48
2 ϕ	40	55-110	0-1	88
3 z	54	100	1	70
3 ϕ	54	110	1	128
4 z	91-127	210	1	104
4 ϕ	91-127	100	1	224
5 z	114-144	210	1	104
5 ϕ	114-144	100	1	265

In order to minimize the material in the acceptance region, the readout electronics are mounted entirely outside the active detector volume. The forward electronics must be mounted in the 10 mm space between the 350 mrad stay-clear space and B1 magnet. This implies that the hybrids carrying the front-end chip must be positioned at an angle of 350 mrad relative to the sensor for the layers 3, 4, and 5 (Figure 17). In the backward direction, the available space is larger and the inner layer electronics can be placed in the sensor plane, allowing a simplified assembly.

The module assembly and the mechanics are quite complicated, especially for the arch modules, and are described in detail elsewhere [34]. The SVT support structure (Figure 16) is a rigid body made from two carbon-fiber cones, connected by a *space frame*, also made of carbon-fiber epoxy laminate.

An optical survey of the SVT on its assembly

jig indicated that the global error in placement of the sensors with respect to design was $\sim 200 \mu\text{m}$, FWHM. Subsequently, the detector was disassembled and shipped to SLAC, where it was re-assembled on the IR magnets. The SVT is attached to the B1 magnets by a set of gimbal rings in such a way as to allow for relative motion of the two B1 magnets while fixing the position of the SVT relative to the forward B1 and the orientation relative to the axis of both B1 dipoles. The support tube structure is mounted on the PEP-II accelerator supports, independently of *BABAR*, allowing for movement between the SVT and the rest of *BABAR*. Precise monitoring of the beam interaction point is necessary, as is described in Section 5.5.

The total active silicon area is 0.96 m^2 and the material traversed by particles is $\sim 4\%$ of a radiation length (see Section 2). The geometrical acceptance of SVT is 90% of the solid angle in the c.m. system, typically 86% are used in charged particle tracking.

5.4. SVT Components

A block diagram of SVT components is shown in Figure 20. The basic components of the detector are the silicon sensors, the *fanout* circuits, the *Front End Electronics* (FEE) and the data transmission system. Each of these components is discussed below.

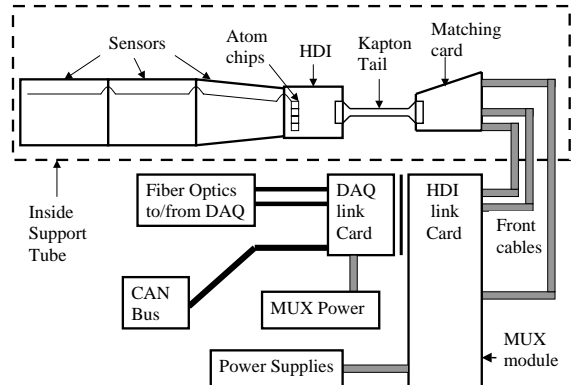


Figure 20. Schematic block diagram showing the different components of the SVT.

5.4.1. Silicon Sensors

The SVT sensors [35] are 300 μm thick double-sided silicon strip devices. They were designed at INFN Pisa and Trieste (Italy) and fabricated commercially [36]. They are built on high-resistivity (6–15 $\text{k}\Omega\text{-cm}$) n-type substrates with p^+ strips and n^+ strips on the two opposite sides. The insulation of the n^+ strips is provided by individual p-stops, so as to achieve an inter-strip resistance greater than 100 $\text{M}\Omega$ at operating bias voltage, normally about 10 V above the depletion voltage.

Typical depletion voltages are in the range 25–35 V. The strips are biased on both sides with polysilicon resistors (4–20 $\text{M}\Omega$) to ensure the required radiation hardness, keeping the voltage drop across resistors and the parallel noise as low as possible. Strips are AC-coupled to the electronics via integrated decoupling capacitors, the capacitance of which depends on the sensor shape, but is always greater than 14 pF/cm. The sensors were designed to maximize the active area, which extends to within 0.7 mm of the physical edges. Another design goal was to control the inter-strip capacitance: values between 0.7 pF/cm and 1.1 pF/cm were obtained for the various sensor shapes. To achieve the required spatial resolution, while keeping the number of readout channels as low as possible, most of the modules have a *floating strip* (*i.e.*, not read out) between two readout strips.

The leakage currents, because of the excellent performance of the manufacturing process, were as low as 50 nA/cm² on average, measured at 10 V above depletion voltage. The silicon sensor parameters have been measured after irradiation with ⁶⁰Co sources. Apart from an increase in the inter-strip capacitance of about 12% during the first 100 krad, the main effect was an increase of the leakage current by 0.7 $\mu\text{A}/\text{cm}^2/\text{MRad}$. However, in a radiation test performed in a 1 GeV/c electron beam, an increase in leakage current of about 2 $\mu\text{A}/\text{cm}^2/\text{MRad}$ and a significant shift in the depletion voltage, dependent on the initial dopant concentration, were observed. A shift of about 8–10 V was seen for irradiation corresponding to a dose of approximately 1 MRad. These observations indicate significant bulk dam-

Table 6

Electrical parameters of the SVT, shown for the different layers and views. C_{input} refers to the total input capacitance, R_{series} is the series resistance. The amplifier peaking time is 200 ns for layers 1–3 and 400 ns for layers 4–5.

Layer/ view	C_{input} (pF)	R_{series} (Ω)	Noise,	
			calc. (elec)	meas. (elec)
1 z	6.0	40.	550	880
1 ϕ	17.2	164.	990	1200
2 z	7.2	48.	600	970
2 ϕ	18.4	158.	1030	1240
3 z	10.5	70.	700	1180
3 ϕ	26.8	230.	1470	1440
4 z	16.6	104.	870	1210
4 ϕ	33.6	224.	1380	1350
5 z	16.6	104.	870	1200
5 ϕ	39.7	265.	1580	1600

age caused by energetic electrons. As indicated by the change in depletion voltage, the SVT sensors could undergo type inversion after about 1–3 MRad. Preliminary tests show that the sensors continue to function after type inversion [37]. Studies of the behavior of SVT modules as a function of radiation dose continue.

5.4.2. Fanout Circuits

The fanout circuits, which route the signals from the strips to the electronics, have been designed to minimize the series resistance and the inter-strip capacitance. As described in ref. [38], a trace on the fanout has a series resistance about 1.6 Ω/cm , an inter-strip resistance $> 20 \text{ M}\Omega$, and an inter-strip capacitance $< 0.5 \text{ pF}/\text{cm}$. The electrical parameters of the final assembly of sensors and fanouts (referred to as *Detector Fanout Assemblies* or DFAs) are summarized in Table 6. Due to the different strip lengths, there are large differences between the inner and the outer layers. Smaller differences are also present between the forward and backward halves of the module, that are of different lengths.

5.4.3. Front End Electronics

The electrical parameters of a DFA and the general *BABAR* requirements are the basic inputs that drove the design of the SVT front-end custom IC; the ATOM (*A Time-Over-Threshold Machine*). In particular, the front-end IC had to satisfy the following requirements:

- signal to noise ratio greater than 15 for *minimum ionizing particle* (MIP) signals for all modules;
- signals from all strips must be retained, in order to improve the spatial resolution through interpolation, while keeping the number of transmitted hits as low as possible. A *hit* refers to a deposited charge greater than 0.95 fC, corresponding to 0.25 MIP;
- the amplifier must be sensitive to both negative and positive charge;
- the peaking time must be programmable, with a minimum of 100 ns (in layers 1 and 2, because of the high occupancy), up to 400 ns (outer layers, with high capacitance);
- capability to accept random triggers with a latency up to 11.5 μ s and a programmable jitter up to ± 1 μ s, without dead time;
- radiation hardness greater than 2.5 MRad;
- small dimensions: 128 channels in a 6.2 mm-wide chip.

These requirements are fully satisfied by the ATOM IC [39], which is depicted schematically in Figure 21.

The linear analog section consists of a charge-sensitive preamplifier followed by a shaper. Gains of 200 mV/fC (low) or 300 mV/fC (high) may be selected. The channel gains on a IC are uniform to 5 mV/fC. Signals are presented to a programmable-threshold comparator, designed so that the output width of the pulse (*Time over Threshold* or ToT) is a quasi-logarithmic function of the collected charge. This output is sampled at 30 MHz and stored in a 193 location buffer. Upon

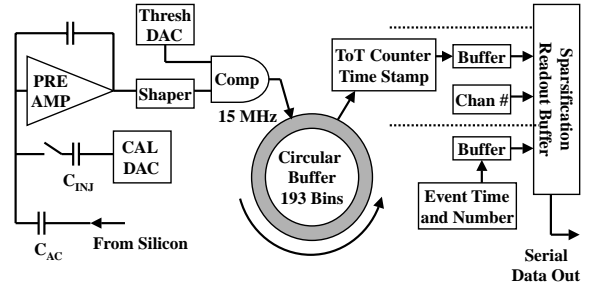


Figure 21. Schematic diagram of the ATOM front end IC.

Table 7

ATOM chip ENC parameters at different peaking times

Peaking time	ENC (0 pF)	Noise slope
100 ns	380 e^-	40.9 e^-/pF
200 ns	280 e^-	33.9 e^-/pF
400 ns	220 e^-	25.4 e^-/pF

receipt of a *Level 1* (L1) trigger, the time and ToT is retrieved from this latency buffer, sparsified, and stored in a four event buffer. Upon the receipt of an *L1 Accept* command from the data acquisition system, the output data (the 4 bits for the ToT, 5 bits for the time stamp, and 7 bits for the strip address) are formatted, serialized, and delivered to the ROM. The IC also contains a test charge injection circuit. The typical noise behavior of the ATOM, as described by the *Equivalent Noise Charge* (ENC) of the linear analog section is given in Table 7.

The average noise for the various module types is shown in Table 6. Given that shot noise due to sensor leakage current is negligible, the expected noise may be calculated from the parameters of Tables 6 and 7. The results of such a calculation are also shown in Table 6. The maximum average noise is 1,600 electrons, leading to a signal-to-noise ratio greater than 15.

The power consumption of the IC is about 4.5 mW/channel. Radiation hardness was studied up to 2.4 MRad with a ^{60}Co source. At that dose, the gain decreased 20%, and the noise increased less than 15%.

The ATOM ICs are mounted on thick-film double-sided hybrid circuits (known as *High Density Interconnects* or HDIs) based on an aluminum-nitride substrate with high thermal conductivity. The electronics are powered through a floating power supply system, in such a way as to guarantee a small voltage drop (< 1 V) across the detector decoupling capacitors.

5.4.4. Data Transmission

The digitized signals are transmitted from the ATOM ICs through a thin *kapton tail* or cable to the *matching cards*, from where they are routed to more conventional cables. Just outside the detector, signals are *multiplexed* by the MUX modules, converted into optical signals and transmitted to the *Readout Modules* (ROMs). The MUX modules also receive digital signals from the DAQ via a fiber optical connection. The SVT is connected to the *BABAR* online detector control and monitoring system via the industry standard CAN bus. Details on SVT data transmission system and DAQ can be found in references [40,41]. Power to SVT modules (silicon sensor bias voltage and ATOM low voltages) is provided by a CAEN A522 power supply system [42].

5.5. Monitoring and Calibration

To identify immediately any operational problems, the SVT is integrated in the control and monitoring system (see Section 12). Major concerns for SVT monitoring are temperature and humidity, mechanical position, and radiation dose.

5.5.1. Temperature and Humidity Monitors

The total power dissipation of the SVT modules is about 350 W, mainly dissipated in the ATOM ICs. External cooling is provided by chilled water at 8°C. In addition, humidity is reduced by a stream of dry air in the support tube.

Since condensation or excessive temperature can permanently damage the FEE, temperature

and humidity monitoring are very important to the safe operation of the SVT. Thermistors are located on the HDIs (for the measurements of FEE temperature), around the SVT, along the cooling systems, and in the electronics (MUX) crates. The absolute temperatures are monitored to 0.2°C and relative changes of 0.1°C. Additionally, a series of humidity sensors are employed to monitor the performance of the dry air system. The temperature and humidity monitors also serve as an interlock to the HDI power supplies.

5.5.2. Position Monitors

A system of capacitive sensors was installed to identify and track changes in the position of the SVT with respect to the PEP-II B1 magnets and the position of the support tube with respect to the DCH. An example of the understanding that can be achieved by this system is given in Figure 22, where the measured changes in the horizontal position of the SVT relative to the DCH are shown for a period of six days in the summer of 1999. These position changes can be attributed to local temperature variations. The sensor data are compared to measurements of the mean position of the interaction point (in the horizontal plane) determined with e^+e^- and $\mu^+\mu^-$ events recorded over this period. While the amplitude of motion at the time was uncharacteristically large, the strong correlation between these independent measurements is quite evident. Alignment with charged particle tracks is now performed routinely to correct for relative motion of the tracking systems, as described in Section 5.6.2.

5.5.3. Radiation Monitors

Radiation monitoring is extremely important to ensure the SVT does not exceed its radiation budget, which could cause permanent damage to the device. To date, the measured radiation absorbed by the SVT is well within the allowed budget.

The monitoring of radiation dose to the SVT is discussed in detail in Section 3.

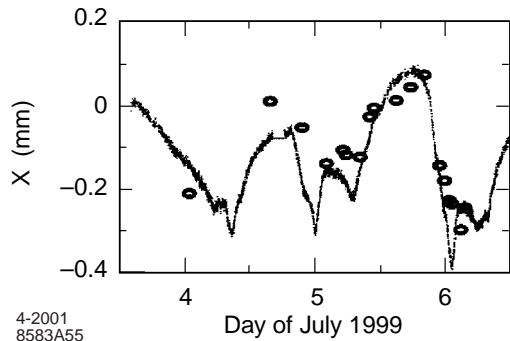


Figure 22. Horizontal motion between the DCH and the support tube measured with the capacitive sensors (curve) compared to the mean x coordinate of the interaction point (circles) measured with e^+e^- and $\mu^+\mu^-$ events over a three-day period in July 1999. An arbitrary offset and scale has been applied to the beam position data.

5.5.4. Calibrations

Once a day, and each time the SVT configuration has changed, calibrations are performed in absence of circulating beams. All electronic channels are tested with pulses through test capacitors, for different values of the injected charge. Gains, thresholds, and electronic noise are measured, and defective channels are identified. The calibration results have proven very stable and repeatable. The main variation in time is the occasional discovery of a new defective channel. The calibration procedures have also been very useful for monitoring noise sources external to the SVT.

5.5.5. Defects

Due to a series of minor mishaps incurred during the installation of the SVT, nine out of 208 readout sections (each corresponding to one side of a half-module) were damaged and are currently not functioning. There is no single failure mode, but several causes: defective connectors, mishandling during installation, and not-fully-understood problems on the FEE hybrid. There has been no module failure due to radiation damage. It should be noted that due to the redundancy afforded by the five layers of the SVT, the presence of the defective modules has minimal impact on physics analyses.

In addition, there are individual channel defects, of various types, at a level of about 1%. Calibrations have revealed an increase in the number of defective channels at a rate of less than 0.2%/year.

5.6. Data Analysis and Performance

This section describes the reconstruction of space points from signals in adjacent strips on both sides of the sensors, the SVT internal and global alignment, single hit efficiency, and resolution and dE/dx performance of the SVT.

5.6.1. Cluster and Hit Reconstruction

Under normal running conditions, the average occupancy of the SVT in a time window of $1\mu\text{s}$ is about 3% for the inner layers, with a significant azimuthal variation due to beam-induced backgrounds, and less than 1% for the outer layers, where noise hits dominate. Figure 23 shows the typical occupancy as a function of IC index (equivalent to azimuthal angle, in this case) for layer 1, ϕ side. In the inner layers, the occupancy is dominated by machine backgrounds, which are significantly higher in the horizontal plane, seen in the plot as the peaks near IC indices 3 and 25.

The first step of the reconstruction program consists in discarding out-of-time channels. A time correction, *i.e.*, the time between the passage of the particle and the time the shaper exceeds threshold, is performed, after which hits with times more than 200 ns from the event time (determined by the DCH) are discarded. The loss of real hits from this procedure is negligible. The resulting in-time hits are then passed to the cluster finding algorithm. First, the charge pulse height (Q) of a single pulse is calculated from the ToT value, and clusters are formed grouping adjacent strips with consistent times. In a second pass, clusters separated by just one strip are merged into one cluster. The two original clusters plus the merged cluster are made available to the pattern recognition algorithm, which chooses among the three.

The position x of a cluster formed by n strips is determined, with the “head-to-tail” algorithm:

$$x = \frac{(x_1 + x_n)}{2} + \frac{p(Q_n - Q_1)}{2(Q_n + Q_1)},$$

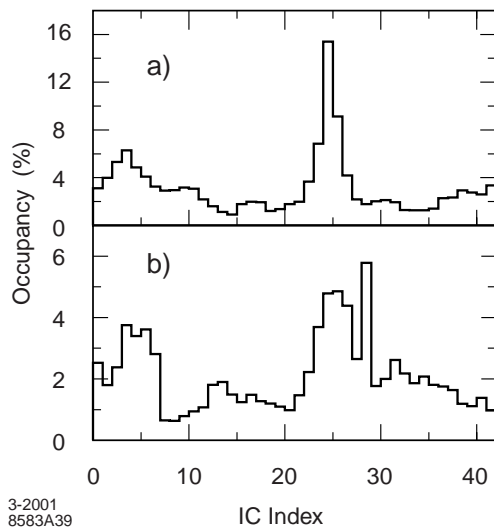


Figure 23. Typical occupancy in percent as a function of IC index in layer 1, ϕ side for a) forward half-modules and b) backward half-modules. The IC index increases with azimuthal angle and the higher occupancy in the horizontal plane is visible near chip indices 3 and 25.

where x_i and Q_i are the position and collected charge of i -th strip, respectively, and p is the read-out pitch. This formula results in a cluster position that is always within $p/2$ of the geometrical center of the cluster. The cluster pulse height is simply the sum of the strip charges, while the cluster time is the average of the signal times.

5.6.2. Alignment

The alignment of the SVT is performed in two steps. The first step consists of determining the relative positions of the 340 silicon sensors. Once this is accomplished, the next step is to align the SVT as a whole within the global coordinate system defined by the DCH. The primary reason for breaking the alignment procedure into these two steps is that the local positions are relatively stable in time compared to the global position. Also, the local alignment procedure is considerably more complex than the global alignment procedure. Thus, the global alignment can be updated on a run-by-run basis, while the local alignment constants are changed as needed, typically

after magnet quenches or detector access.

The local alignment procedure is performed with tracks from $e^+e^- \rightarrow \mu^+\mu^-$ events and cosmic rays. Well isolated, high momentum tracks from hadronic events are also used to supplement di-muon and cosmic data. Data samples sufficient to perform the local alignment are collected in one to two days of typical running conditions.

In $\mu^+\mu^-$ events, the two tracks are simultaneously fit using a Kalman filter technique and the known beam momentum. The use of tracks from cosmic rays reduces any systematic distortion that may be introduced due to imprecise knowledge of the beam momenta. No information from the DCH is used, effectively decoupling the SVT and DCH alignment.

In addition to the information from tracks, data from an optical survey performed during the assembly of the SVT are included in the alignment procedure. The typical precision of these optical measurements is $4\mu\text{m}$. This survey information is only used to constrain sensors relative to other sensors in the same module, but not one module to another or one layer to another. Furthermore, only degrees of freedom in the plane of the sensor are constrained as they are expected to be the most stable, given the assembly procedure.

Using the hit residuals from the aforementioned set of tracks and the optical survey information, a χ^2 is formed for each sensor and minimized with respect to the sensor's six local parameters. The constraints coming from the overlapping regions of the silicon sensors, the di-muon fit, the cosmic rays, and the optical survey result in internally consistent local alignment constants.

Figure 24 shows a comparison between the optical alignment made during the SVT assembly in February 1999 and a local alignment using data taken during January 2000. The alignment from tracking data was made without using cosmics or constraints from the optical survey. The width of the distributions in these plots has four contributions: 1) displacement during the transfer of the SVT from the assembly jig to the IR magnets, 2) time dependent motion of the SVT after mounting, 3) statistical errors, and 4) systematic errors. The second set of plots shows the difference in two alignment sets for data taken in January 2000 as

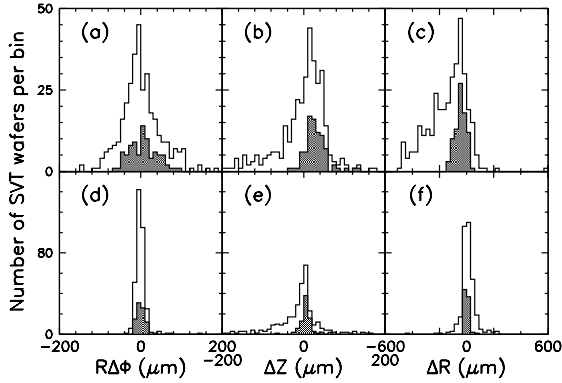


Figure 24. Comparison of a local alignment of all the sensors in the SVT using data from January 2000 with the optical survey of the SVT made during assembly in February 1999 in the (a) $r\Delta\phi$, (b) Δz and (c) Δr coordinates. Plots (d), (e), and (f) show the difference between two local alignments using data from January 15-19 and March 6-7, 2000 for the $r\Delta\phi$, Δz , and Δr coordinates, respectively. In all the plots, the shaded regions correspond to the sensors in the first three layers. In comparing the different alignments and optical survey, a six parameter fit (three global translations and three global rotations) has been applied between the data sets.

compared to March 2000. In general, the stability of the inner three layers is excellent, with slightly larger tails in the outer two layers. The radial coordinate is less tightly constrained in all measurements because the radial location of the charge deposition is not well known, and most of the information about the radial locations comes only from constraints in the overlap region of the sensors.

After the internal alignment, the SVT is considered as a rigid body. The second alignment step consists in determining the position of the SVT with respect to the DCH. Tracks with sufficient numbers of SVT and DCH hits are fit two times: once using only the DCH information and again using only the SVT hits. The six global alignment parameters, three translations and three rotations, are determined by minimizing the difference between track parameters ob-

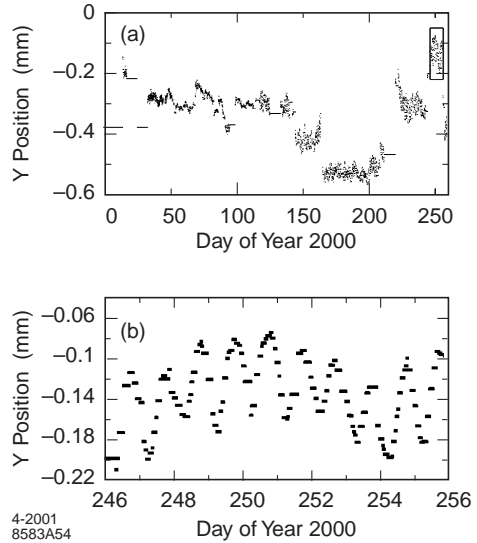


Figure 25. Global alignment of the SVT relative to the DCH based on e^+e^- and $\mu^+\mu^-$ events: changes in the relative vertical placement measured a) over the entire ten-month run in the year 2000, and b) a ten-day period, illustrating diurnal variations.

tained with the SVT-only and the DCH-only fits. As reported above, because of the diurnal movement of the SVT with respect to the DCH, this global alignment needs to be performed once per run (\sim every 2-3 hours). The alignment constants obtained in a given run are then used to reconstruct the data in the subsequent run. This procedure, known as *rolling calibration*, ensures that track reconstruction is always performed with up-to-date global alignment constants.

A record of the changes in the relative position of the SVT as determined by *rolling calibrations* is shown in Figure 25. The position is stable to better than $\pm 100 \mu\text{m}$ over several weeks, but changes abruptly from time to time, for instance, during access to the detector. The calibrations track diurnal variations of typically $\pm 50 \mu\text{m}$ that have been correlated with local changes in temperature of about $\pm 2^\circ\text{C}$. Movements within a single run are small compared to the size of the beam.

5.6.3. Performance

The SVT efficiency can be calculated for each half-module by comparing the number of associated hits to the number of tracks crossing the active area of the module. As can be seen in Figure 26, a combined hardware and software efficiencies of 97% is measured, excluding defective readout sections (9 out of 208), but employing no special treatment for other defects, such as broken AC coupling capacitors or dead channels on front-end chips. Actually, since most of the

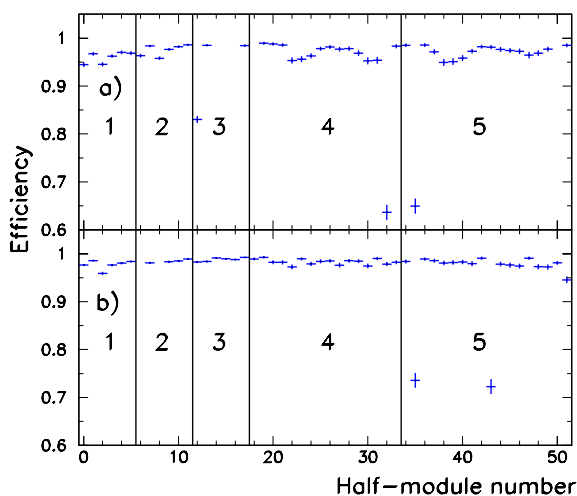


Figure 26. SVT hit reconstruction efficiency, as measured on $\mu^+\mu^-$ events for a) forward half-modules and b) backward half-modules. The plots show the probability of associating both a ϕ and z hit to a track passing through the active part of the detector. The horizontal axis corresponds to the different modules, with the vertical lines separating the different layers as numbered. Missing values correspond to non-functioning half-modules.

defects affect a single channel, they do not contribute to the inefficiency, because most tracks deposit charge in two or more strips due to track crossing angles, and charge diffusion.

The spatial resolution of SVT hits is determined by measuring the distance (in the plane of the sensor) between the track trajectory and the hit, using high-momentum tracks in two prong

events. The uncertainty due to the track trajectory is subtracted from the width of the residual distribution to obtain the hit resolution. Figure 27 shows the SVT hit resolution for z and ϕ side hits as a function of track incident angle, for each of the five layers. The measured resolutions are in excellent agreement with expectations from Monte Carlo simulations.

Initial studies have shown that hit reconstruction efficiency and spatial resolution are effectively independent of occupancy for the occupancy levels observed so far.

Measurement of the ToT value by the ATOM ICs enables one to obtain the pulse height, and hence the ionization dE/dx in the SVT sensor. The values of ToT are converted to pulse height using a lookup table computed from the pulse shapes obtained in the bench measurements. The pulse height is corrected for track length variation. The double-sided sensors provide up to ten measurements of dE/dx per track. For every track with signals from at least four sensors in the SVT, a 60% truncated mean dE/dx is calculated. The cluster with the smallest dE/dx energy is also removed to reduce sensitivity to electronics noise. For MIPs, the resolution on the truncated mean dE/dx is approximately 14%. A 2σ separation between the kaons and pions can be achieved up to momentum of 500 MeV/c, and between kaons and protons beyond 1 GeV/c.

5.7. Summary and Outlook

The SVT has been operating efficiently since its installation in the *BABAR* experiment in May 1999. The five layer device, based on double-sided silicon sensors, has satisfied the original design goals, in particular the targets specified for efficiency, hit resolution, and low transverse momentum track reconstruction. The radiation dose during the first 25 fb^{-1} of integrated luminosity is within the planned budget, and no modules have failed due to radiation damage. The performance of the SVT modules at high radiation dose is currently being studied. Early results indicate that the sensors will continue to function after type inversion (at 1–3 MRad), but further tests with irradiated sensors and ATOM ICs need to be performed. A program of spare module production

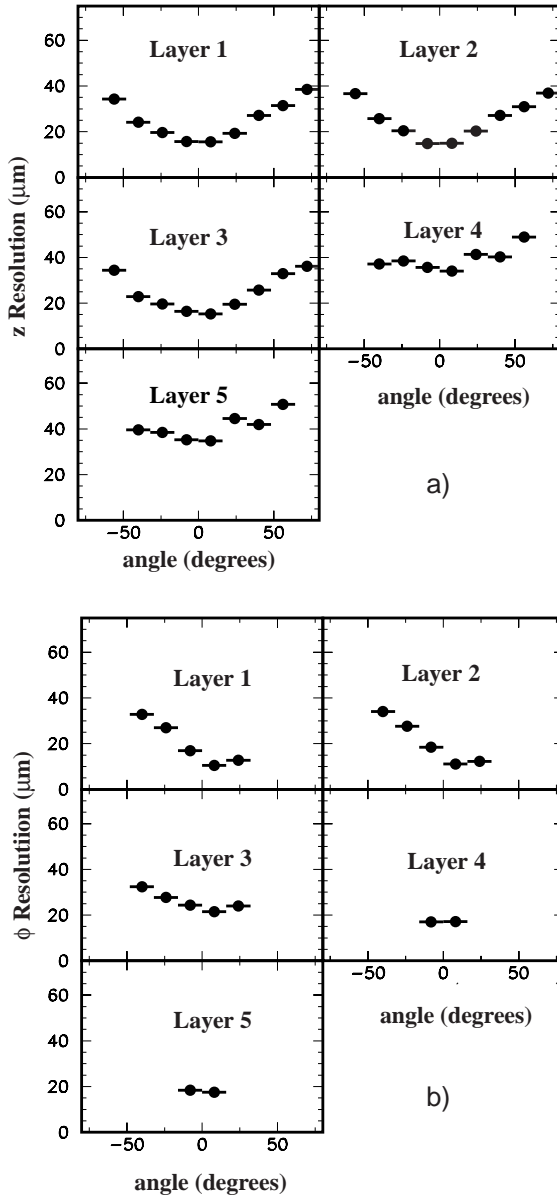


Figure 27. SVT hit resolution in the a) z and b) ϕ coordinate in microns, plotted as a function of track incident angle in degrees. Each plot shows a different layer of the SVT. The plots in the ϕ coordinate for layers 1-3 are asymmetric around $\phi = 0$ because of the “pinwheel” design of the inner layers. There are fewer points in the ϕ resolution plots for the outer layers as they subtend smaller angles than the inner layers.

has commenced, with the goal of replacing modules that are expected to fail due to radiation damage. Beam-generated backgrounds are expected to rise with increasing luminosity. Physics studies at five times the current backgrounds levels indicate no change in mass or vertex resolution for the mode $B^0 \rightarrow J/\psi K_S^0$ and a $\sim 20\%$ loss of resolution in the $D^{*+} - D^0$ mass difference. In this study the detector efficiency for both decay modes was lower by 15-20%.